OPTICAL WAVEFRONT ENGINEERING OF PEROVSKITE LIGHT EMISSION BY METASTRUCTURES

A Thesis

by

YIXIN CHEN

Submitted to the Graduate and Professional School of
Texas A&M University
in partial fulfillment of the requirements for the degree of

MASTER OF SCIENCE

Chair of Committee,	Zi Jing Wong
Committee Members,	Mohammad Naraghi
	Shoufeng Lan
Head of Department,	Srinivas Rao Vadali

August 2021

Major Subject: Aerospace Engineering

ABSTRACT

The demand for programmable, low-cost, compact and multifunctional lighting sources is critical for the advances of next-generation optoelectronic devices. Among light-emitting materials, halide perovskites materials have gained tremendous attention in recent years in a wide range of applications, such as high-efficient solar cells, light emitting diodes (LEDs), and lasers, due to their exotic properties such as long-carrier diffusion length, low defect density and controllable bandgaps, low-cost and easy processing, and high photoluminescence quantum yield. However, direct control of light emission pattern has not yet been explored. In this thesis research, direct control of light emission from $MAPbI_3$ lead halide perovskite using dielectric metasurfaces is experimentally investigated. Several devices, including perovskite directional emitter, perovskite self-focusing lens, and perovskite vortex beam generator, are verified through numerical simulations. Experimentally, a perovskite directional emitter device is fabricated and measured through optical measurements. The direct and on-demand perovskite light emission pattern control will facilitates its broader applications in light raging, directional LED, self-focusing perovskite lens, beam steering, and free-space optical communications, etc.

ACKNOWLEDGEMENTS

The three years in graduate school have been an incredible journey for me. All the hard work, frustration, mistakes, excitements, and accomplishments have prepared me into a better student, a more-versed researcher, and most importantly, a better person. During this journey, I have received overwhelming help from many people, whom I would like to acknowledge here gratefully.

First of all, I would like to thank my advisor Dr. Wong. He gave me the wonderful opportunity to explore the fields of nanophotonics and metamaterials. He has guided me through every step of my progress, offered me with countless suggestions, and enriched and motivated me with his ultimate passion and insatiable curiosity to science. I will always be grateful for his support along the road.

My committee members, Dr. Naraghi and Dr. Lan have always been supportive to me. Part of my work has been done in Dr. Lan's lab, for which I am very grateful of. I would like to thank Dr. Xuezhi Ma, for his help in optical measurements and endless scientific discussions.

Working with many of my labmates and colleagues has always been enjoyable. I would like to thank Dr. Bin Ai, who was my first labmate and friend in College Station, for his help during my first year. It has been great fun to work with Ziwei Fan and Jinze Cai, with whom I spend the most time and shared the greatest amount of jokes over these three years. I would also like to thank Dr. Chengzhi Qin for expanding my knowledge in physics and photonics. Staff members in AggieFab, especially Dr. Ming-Wei Lin, Larry

Rehn and Ethan Morse, have offered me wonderful assistance over the years. Other friends in our lab, including Jitesh, Victor, Sam, and Naga have all been very helpful to me.

I would like to thank my friends in College Station and other parts of the United States, especially Fubiao Zhen, Pengyang Li, Botao Chen, and Ruoyang Yan, for all the laugh we've had, for listening to my endless complaints, and for always having me back.

I owe the greatest gratitude to my parents, for their endless and unconditional support, and for my absence from home for so many years.

CONTRIBUTORS AND FUNDING SOURCES

Contributors

This work was supervised by a thesis committee consisting of Professor Zi Jing Wong and Professor Mohammad Naraghi of the Department of Aerospace Engineering and Professor Shoufeng Lan of the Department of Mechanical Engineering.

The perovskite precursor and perovskite thin films were prepared by Jinze Cai of the Department of Materials Science and Engineering. The optical setup depicted in Chapter 3 were built by and optical measurements were conducted in part by Dr. Xuezhi Ma of the Department of Mechanical Engineering.

All other work conducted for the thesis was completed by the student independently.

Funding Sources

The graduate study was supported by NASA Grant (80NSSC18P2146), President's Excellence Fund (T3 and X-Grant), and TAMU Start-up Fund.

TABLE OF CONTENTS

Page

LIST OF FIGURES

Page

LIST OF TABLES

Page

CHAPTER I

INTRODUCTION

This chapter starts with a brief introduction on the light (wave) propagation and concepts of optical wavefront and phases. Then, metasurfaces that are used to locally control the phase of propagating plane waves will be briefly introduced and reviewed, with focuses on its mechanisms. Finally, the outline of the thesis will be introduced.

Optical Wavefront

A linearly polarized external light can be considered as electromagnetic plane wave propagation, whose 3D animation is shown in Figure 1a. In Figure 1a, the red and blue arrows indicate the electric field (*E*-field) magnitude and direction, which can be considered as the polarization directions. The black arrow indicates the wavevector $\boldsymbol{k}$, representing the wave propagation direction. The red and blue planes are planes of constant phases, which are defined as optical wavefront [1].

Figure 1b shows a simplified 2D model of Figure 1a, in which the red and blue lines indicate planes of constant phases, or wavefronts. The red arrow indicates wave propagation direction $\boldsymbol{k}$. Notably, the phase different $\Delta\varphi$ between adjacent lines of each color is 2π. The essence of metasurfaces is to control

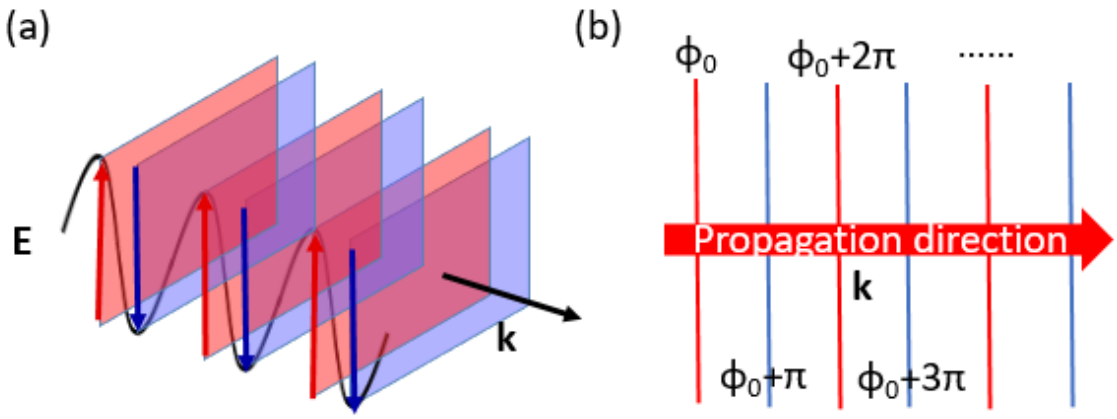

Figure 1. (a) 3D and (b) 2D illustration of plane wave propagation and optical wavefronts.

Metasurfaces for Wavefront Control

Since their early discoveries, optical metamaterials have attracted tremendous attention in achieving exotic optical properties such as zero or negative refractive index [2, 3], extraordinary transmission [4, 5], negative permeability [6, 7], etc. Metamaterials are man-made subwavelength nanostructures to demonstrate novel properties, phenomena, or functions that otherwise cannot been attainable through existing materials. As two-dimension counterparts of metamaterials, phase-gradient metasurfaces are ultrathin (<1μm thickness) spatially-varying sub-wavelength meta-atoms that are arranged to locally manipulate the wavefront of propagating plane waves [8-10]. The main difference between phase-gradient metasurfaces and metamaterials is that phase-gradient metasurfaces manipulate light locally at each sub-wavelength point, while in most cases, metamaterials attain global exotic optical properties. In recent decade, optical metasurfaces enabled novel functionalities such as beam steering [11, 12], ultrathin

metalens [13-15], orbital angular momentum generation [16-18], etc. Due to their unique ability to locally and arbitrarily control the propagating phase of an incoming wave, metasurfaces have rapidly emerged to advance devices such as broadband achromatic metalenses [19-21], ultrathin invisibility cloaks [22, 23], metasurface holography [24-26], image processors [27, 28], etc.

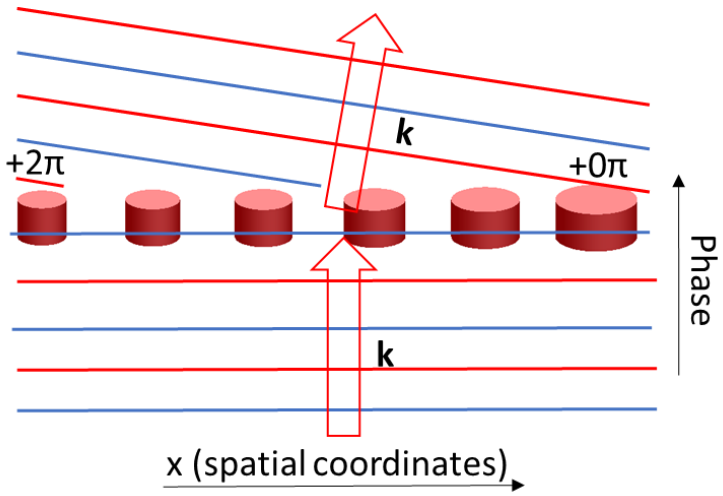

Figure 2. Illustration of an array of spatially varying dielectric cylinders imposing gradient phase delay to an incident plane wave.

It is important to understand how metasurfaces utilize spatial-varying structures to locally manipulate the optical wavefronts. As shown in Figure 2, a plane wave with wavevector ***k*** is impinging on an array of metasurface, which is consisted of 6 spatially varying sub-wavelength cylinders made of high-index dielectric materials surrounded in a low refractive index environment (usually air or water). The blue and red lines indicate the wavefront of light propagation. When the incident plane wave transmit through the sub-wavelength cylinders, cylinders of different sizes give different propagating phase delay to the plane wave, with the largest cylinder giving the greatest amount of phase

delay, and vice versa. When the phase delays imposed by the 6 cylinders gradually changes within 2π, an anomalous refraction of the incident plane wave is achieved.

Other types of metasurfaces apply similar concepts but different spatial phase distribution to locally impose phase delays to external light, in order to get different functions. As Figure 3 shows some examples of the different functions attained by phase-gradient metasurfaces. In Figure 3a, a high-resolution ultrathin dielectric (TiO_2) metalens has been designed and fabricated. The metalens has a high numerical aperture (NA) of 0.8, high magnification (170x) and high efficiency (88% for 405 nm light) [29]. Its focusing effect has been experimentally measured, which is shown in Figure 3b. Since then, high-efficiency achromatic broadband metalenses [30-32] and tunable metalenses [33, 34]. In Figure 3c and 3d, a high efficiency (> 80%) metasurface hologram has been constructed [35] with broad operation band from 650 nm to 1080 nm wavelength. Ultrathin metasurface holograms have since then been enriched with more functionalities, such as programmable holograms [36], multi-color 3D meta-holography [37], 3D orbital angular momentum holography [38], and metasurface holography for encryption and secret sharing [39-42].

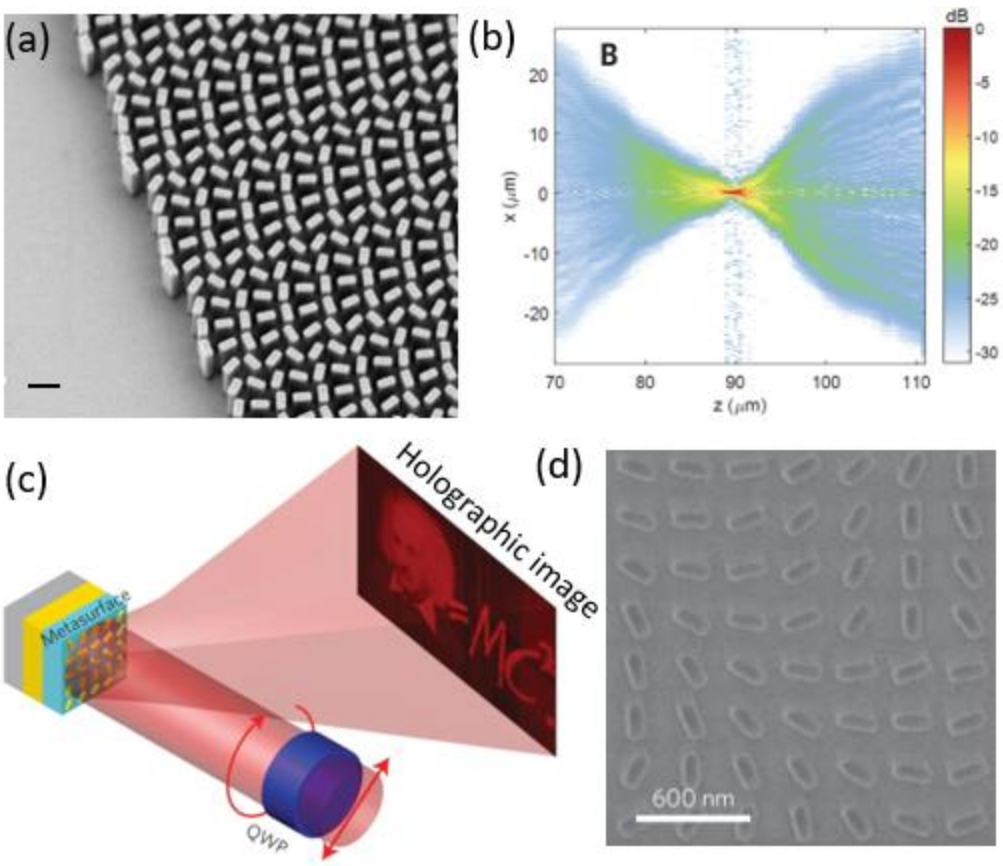

Figure 3. Metasurfaces enabling multifunctional control of external light. (a) SEM image of an ultrathin dielectric metalens. Scale bar is 300nm. (b) Measured focusing intensity distribution of the dielectric metalens. A focusing effect at the design focal length (f = 90 μm) (c) Illustration of a high efficiency reflective metasurface hologram. In the inset, the measured holographic image is shown. (d) SEM image of part of the metasurface hologram. (a) and (b) Reproduced with permission from ref. [29] Copyright (2016) American Association for the Advancement of Science; (c) and (d) Reproduced with permission from ref. [35] Copyright (2015) Nature Publishing Group.

Thesis Outline

This thesis contains the motivation, concept, design, simulations, fabrication, and the measurement of a series of perovskite-based metastructures that allow the local and

arbitrary wavefront control of the light emission from lead halide perovskites. Specifically, the thesis will be outlined as follows:

In Chapter 2, several techniques using nanostructures to control the light emission from nanomaterials and quantum dots will be firstly reviewed, including the used of Yagi-Uda antenna arrays, and symmetric-broken nanorod arrays. Then, halide perovskites will be introduced, and the advantages and qualities of lead halide perovskites used as novel light sources will be highlighted. Detailed explanation on how to use metasurfaces to control light emission by coupling light emission into resonant cavities will be then discussed. Simulations of three devices, including perovskite directional emitter, self-focused perovskite lens, as well as perovskite vortex beam generator will be discussed.

Chapter 3 will focus on the specific design, fabrication and measurement of a perovskite directional emitter. First, the design of resonant Bragg cavity and silicon metasurface will be discussed. Then, the fabrication process of the perovskite emitter will be then illustrated, with emphasis on the optimization of the fabrication process in order to keep the perovskite layer protected. Finally, the optical measurement of the perovskite directional emitter will be discussed.

Finally, in Chapter 4, some conclusion remarks will be discussed. Outlooks including the future realization of self-focused perovskite emitting lens will be presented.

References

[1] Hecht, Eugene, and Alfred Zajac. Optics. Vol. 4. San Francisco: Addison Wesley, 2002.

[2] Valentine, Jason, et al. "Three-dimensional optical metamaterial with a negative refractive index." Nature 455.7211 (2008): 376-379.

[3] Zhang, Shuang, et al. "Negative refractive index in chiral metamaterials." Physical review letters 102.2 (2009): 023901.

[4] Rodrigo, Sergio G., Fernando de Leon-Perez, and Luis Martín-Moreno. "Extraordinary optical transmission: fundamentals and applications." Proceedings of the IEEE 104.12 (2016): 2288-2306.

[5] Xu, Hao, et al. "Effective-medium models and experiments for extraordinary transmission in metamaterial-loaded waveguides." Applied Physics Letters 92.4 (2008): 041122.

[6] Zhao, Qian, et al. "Electrically tunable negative permeability metamaterials based on nematic liquid crystals." Applied physics letters 90.1 (2007): 011112.

[7] Lapine, Mikhail, Ilya Shadrivov, and Yuri Kivshar. "Wide-band negative permeability of nonlinear metamaterials." Scientific reports 2.1 (2012): 1-4.

[8] Yu, Nanfang, and Federico Capasso. "Flat optics with designer metasurfaces." Nature materials 13.2 (2014): 139-150.

[9] Yu, Nanfang, et al. "Light propagation with phase discontinuities: generalized laws of reflection and refraction." science 334.6054 (2011): 333-337.

[10] Chen, Hou-Tong, Antoinette J. Taylor, and Nanfang Yu. "A review of metasurfaces: physics and applications." Reports on progress in physics 79.7 (2016): 076401.

[11] Wei, Zeyong, et al. "Highly efficient beam steering with a transparent metasurface." Optics express 21.9 (2013): 10739-10745.

[12] Wu, Pin Chieh, et al. "Dynamic beam steering with all-dielectric electro-optic III–V multiple-quantum-well metasurfaces." Nature communications 10.1 (2019): 1-9.

[13] West, Paul R., et al. "All-dielectric subwavelength metasurface focusing lens." Optics express 22.21 (2014): 26212-26221.

[14] Wang, Shuming, et al. "A broadband achromatic metalens in the visible." Nature nanotechnology 13.3 (2018): 227-232.

[15] Chen, Ke, et al. "A reconfigurable active huygens' metalens." Advanced materials 29.17 (2017): 1606422.

[16] Li, Yang, et al. "Orbital angular momentum multiplexing and demultiplexing by a single metasurface." Advanced Optical Materials 5.2 (2017): 1600502.

[17] Ren, Haoran, et al. "Metasurface orbital angular momentum holography." Nature communications 10.1 (2019): 1-8.

[18] Guo, Yinghui, et al. "Merging geometric phase and plasmon retardation phase in continuously shaped metasurfaces for arbitrary orbital angular momentum generation." Acs Photonics 3.11 (2016): 2022-2029.

[19] Ndao, Abdoulaye, et al. "Octave bandwidth photonic fishnet-achromatic-metalens." Nature communications 11.1 (2020): 1-6.

[20] Chen, Wei Ting, et al. "A broadband achromatic metalens for focusing and imaging in the visible." Nature nanotechnology 13.3 (2018): 220-226.

[21] Ni, Xingjie, et al. "An ultrathin invisibility skin cloak for visible light." Science 349.6254 (2015): 1310-1314.

[22] Chu, Hongchen, et al. "A hybrid invisibility cloak based on integration of transparent metasurfaces and zero-index materials." Light: Science & Applications 7.1 (2018): 1-8.

[23] Ni, Xingjie, Alexander V. Kildishev, and Vladimir M. Shalaev. "Metasurface holograms for visible light." Nature communications 4.1 (2013): 1-6.

[24] Zheng, Guoxing, et al. "Metasurface holograms reaching 80% efficiency." Nature nanotechnology 10.4 (2015): 308-312.

[25] Li, Lianlin, et al. "Electromagnetic reprogrammable coding-metasurface holograms." Nature communications 8.1 (2017): 1-7.

[26] Li, Lianlin, et al. "Machine-learning reprogrammable metasurface imager." Nature communications 10.1 (2019): 1-8.

[27] Cordaro, Andrea, et al. "High-index dielectric metasurfaces performing mathematical operations." Nano letters 19.12 (2019): 8418-8423.

[28] Zhou, You, et al. "Flat optics for image differentiation." Nature Photonics 14.5 (2020): 316-323.

[27] Chen, Xianzhong, et al. "Dual-polarity plasmonic metalens for visible light." Nature communications 3.1 (2012): 1-6.

[28] Ni, Xingjie, et al. "Ultra-thin, planar, Babinet-inverted plasmonic metalenses." Light: Science & Applications 2.4 (2013): e72-e72.

[29] Khorasaninejad, Mohammadreza, et al. "Metalenses at visible wavelengths: Diffraction-limited focusing and subwavelength resolution imaging." Science 352.6290 (2016): 1190-1194.

[30] Chen, Wei Ting, et al. "A broadband achromatic metalens for focusing and imaging in the visible." Nature nanotechnology 13.3 (2018): 220-226.

[31] Wang, Shuming, et al. "A broadband achromatic metalens in the visible." Nature nanotechnology 13.3 (2018): 227-232.

[32] Ndao, Abdoulaye, et al. "Octave bandwidth photonic fishnet-achromatic-metalens." Nature communications 11.1 (2020): 1-6.

[33] Arbabi, Ehsan, et al. "MEMS-tunable dielectric metasurface lens." Nature communications 9.1 (2018): 1-9.

[34] Chen, Ke, et al. "A reconfigurable active huygens' metalens." Advanced materials 29.17 (2017): 1606422.

[35] Zheng, Guoxing, et al. "Metasurface holograms reaching 80% efficiency." Nature nanotechnology 10.4 (2015): 308-312.

[36] Li, Lianlin, et al. "Electromagnetic reprogrammable coding-metasurface holograms." Nature communications 8.1 (2017): 1-7.

[37] Li, Xiong, et al. "Multicolor 3D meta-holography by broadband plasmonic modulation." Science advances 2.11 (2016): e1601102.

[38] Ren, Haoran, et al. "Complex-amplitude metasurface-based orbital angular momentum holography in momentum space." Nature Nanotechnology 15.11 (2020): 948-955.

[39] Zhou, Hongqiang, et al. "Polarization-encrypted orbital angular momentum multiplexed metasurface holography." ACS nano 14.5 (2020): 5553-5559.

[40] Georgi, Philip, et al. "Optical secret sharing with cascaded metasurface holography." Science Advances 7.16 (2021): eabf9718.

[41] Wu, Jun Wei, et al. "Full‐State Synthesis of Electromagnetic Fields using High Efficiency Phase‐Only Metasurfaces." Advanced Functional Materials 30.39 (2020): 2004144.

[42] Li, Jianxiong, et al. "Addressable metasurfaces for dynamic holography and optical information encryption." Science advances 4.6 (2018): eaar6768.

CHAPTER II

DESIGN OF PEROVSKITE-BASED METASTRUCTURES FOR LIGHT EMISSION WAVEFRONT CONTROL

This chapter focuses on how control the light emission from nanomaterials using nanostructures. First, we begin by reviewing some typical techniques to use nanostructure arrays to control the directionality of nanomaterials spontaneous light emission, including the use of Yagi-Uda antenna arrays, and symmetry-broken nanorod arrays. Then, we will discuss how to use metasurfaces to achieve arbitrary wavefront control of nanomaterial light emission. Specifically, two types of cavities, including photonic crystal cavities and closed cavities are identified to achieve directionality for light emission. Then, arbitrary wavefront control of light emission can be achieved by introducing metasurfaces. Lead halide perovskites will be then introduced, with emphasis on its many advantages to be used as novel nanomaterial light sources. By the use of closes cavities and metasurfaces, arbitrary wavefront control of perovskite light emission can be achieved. Several novel perovskite light emission patterns can be attained, including perovskite directional emitter, self-focused perovskite lens, as well as perovskite vortex beam generator will be discussed.

Light Emission Pattern Control Using Nanostructures

On-demand light emission pattern control has drawn immense attention in pursuing multifunctional, programmable, and smart next generation light sources. In

recent decades, with the development of micro/nanofabrication techniques, researchers have been exploring nanostructures to control the light emission patterns from nanomaterials. Nanoscale Yagi-Uda antennae have been used to control the light emission of quantum dots and nanomaterials [1]. Yagi-Uda antenna is a common concept for radio-frequency (RF) community, in order to control the directionality of the transmission of radio waves. The same concept has been applied in the optical regime to control the light emission directionality from quantum dots. Yagi-Uda antenna array, which consists of a driver element, a reflector and several directors, with the number and spacing of directors controlling the directionality of the transmitted radio waves, as shown in Figure 4a and 4b. Over the years, more advanced structures and functions have been realized, such as three-dimensional Yagi-Uda antenna array [2], Babinet-inverted Yagi-Uda antenna array [3], hybrid metal-dielectric Yagi-Uda antennae arrays [4, 5], actively tunable Yagi-Uda antenna arrays for reconfigurable radiation patterns [6-8].

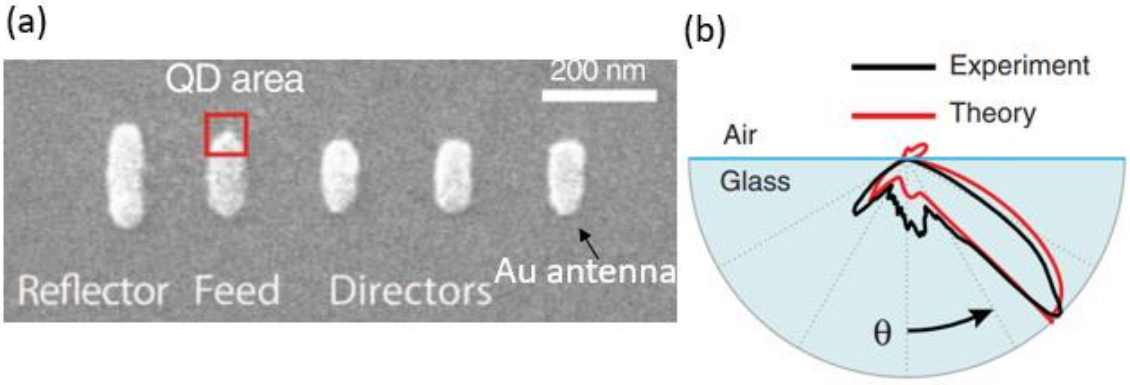

Figure 4. Light emission directionality control by non-uniform nanostructures. (a) Control of quantum dot light emission using Yagi-Uda antenna. (b) Measured directional emission from quantum dots with directionality control from Yagi-Uda antenna array. (a) and (b) Reproduced with permission from ref. [1] Copyright (2010) American Association for the Advancement of Science.

Another typical approach to control light emission is the use of symmetry-broken nanorod arrays. In one example, a symmetry-broken III-V light-emitting nanorod array was patterned [9]. The light emission pattern was measured and directional light emission has been observed. Other symmetric-broken structures have also been used to control the directionality of light emission [10-13].

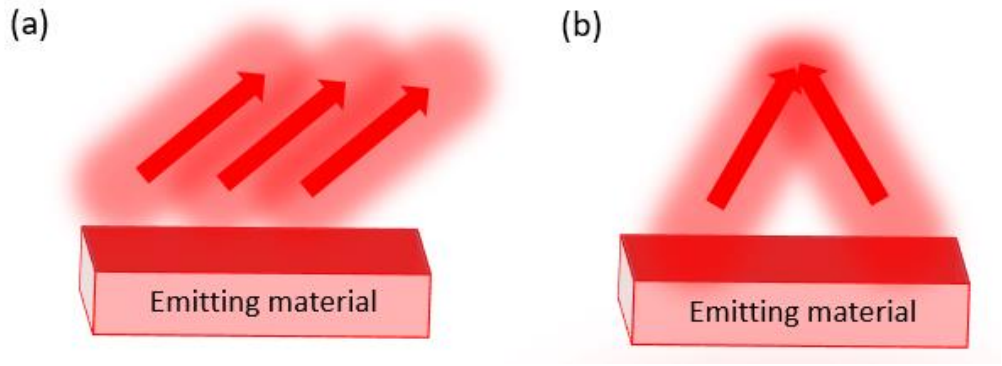

Figure 5. Illustration of (a) directional emission and (b) self-focused emission from a light-emitting nanomaterial.

In both ways to control light emission from nanomaterials or quantum dots, only directionality of light emission can be engineered (Figure 5a). This is because in both cases, it is not the local wavefront at each subwavelength point that is being engineered. In order to get any arbitrary light emission pattern, for instance, self-focused emission (Figure 5b), more universal approach needs to be developed. It is of our best interest to locally change the light emission wavefront of each subwavelength position, in order to get the optimized ability to control the wavefront of light emission.

Metasurface Controlling Light Emission Pattern

As a versatile and universal way to control the optical wavefront of external light, phase-gradient metasurfaces can be utilized as a good way to manipulate light emission pattern [14, 15]. Comparing to external light (Figure 6a), the difficulty to manipulate light emission using metasurfaces is due to the lack of directionality (Figure 6b). In order to attain the control of light emission using metasurface, directionality can be acquired by coupling light-emitting material in a cavity. As two examples, two types of cavities are shown in Figure 6. In Figure 6c, a thin layer of light-emitting material sitting on a substrate is patterned as a photonic crystal cavity. By forming a photonic crystal cavity, directionality from the light emission can be attained along the in-plane directions. By introducing spatially-varying structures of different sizes, light emission pattern can subsequently manipulated [14], as shown in Figure 6e-g. In Figure 6e, indium gallium nitride (InGaN) quantum wells (QWs) embedded in gallium nitride (GaN). The GaN layer is patterned in a period such that the nanostructure array reaches a photonic crystal cavity. Effectively, the photonic structure cavity restricted the light emission from the InGaN QW in the in-plane direction (i.e., $\boldsymbol{k}_x$). After that, by patterning the nanostructure with different sizes (shown in the top-view SEM image in Figure 6f), different amounts of phases delay are assigned locally for each position. When the phase is applied with a constant gradient, a directional light emission can be achieved, which is shown in the measured far-field emission pattern in Figure 6g. Another approach utilizes a closed resonant cavity (Fabry-Perot cavity or Bragg cavity) [15], by sandwiching a light emitting layer in-between two reflecting mirrors. When the distance between the two mirrors is carefully adjusted

facilitating a resonance condition, directionality along the out-of-plane direction can be attained (i.e. $\boldsymbol{k}_z$). By placing another layer of metasurfaces on top of either mirror, manipulating the light emission pattern is then achievable, as shown in Figure 6h and 6i. In Figure 6h, a GaN based LED is sandwiched in between two metallic mirrors. Another metasurface is fabricated on top the one of the metallic mirror. By design the metasurface such that it imposes a constant phase gradient to the incident light, a directional emission from the GaN-based LED can be achieved. Figure 6i shows the measured far-field radiation pattern of the GaN-based LED embedded in the closed cavity with metasurfaces on top, and a directional emission can be seen. It is important to note that, the cavity has to operate in the resonant condition, such that the directionality can be best attained. Therefore, optimizing the dimensions of the cavity is essential. For the photonic crystal cavity, the periodicity of the photonic crystal needs to be optimized. For the closed cavity (Fabry-Perot cavity or Bragg cavity), the distance between the two mirrors needs to be optimized.

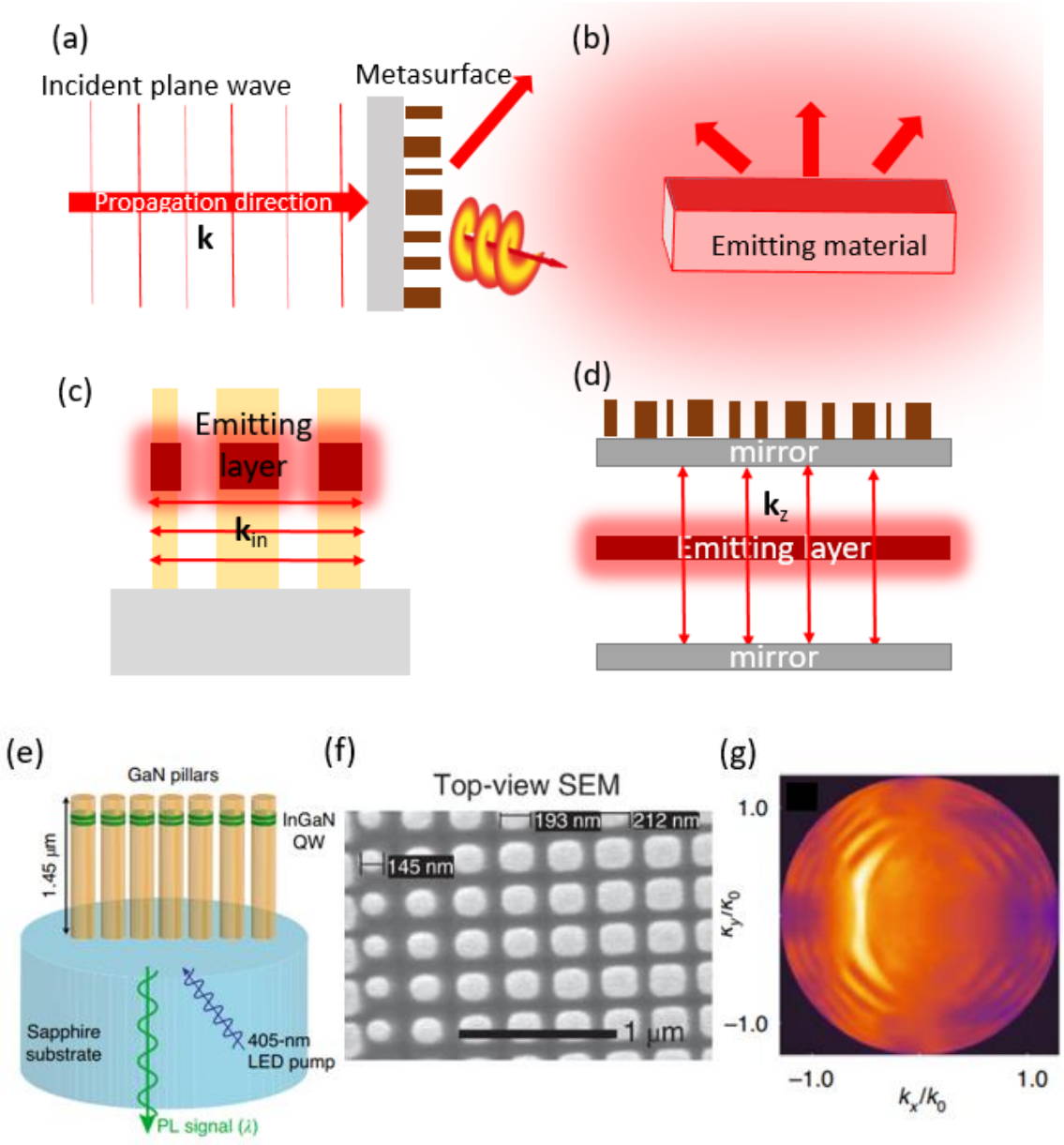
(a)
Incident plane wave
Metasurface
Propagation direction
k
(b)
Emitting material
(c)
Emitting layer
k_{in}
(d)
mirror
k_z
Emitting layer
mirror
(e)
GaN pillars
InGaN QW
1.45 μm
Sapphire substrate
405-nm LED pump
PL signal (λ)
(f)
Top-view SEM
193 nm
212 nm
145 nm
1 μm
(g)
1.0
k_y/k_0
−1.0
−1.0
1.0
k_x/k_0

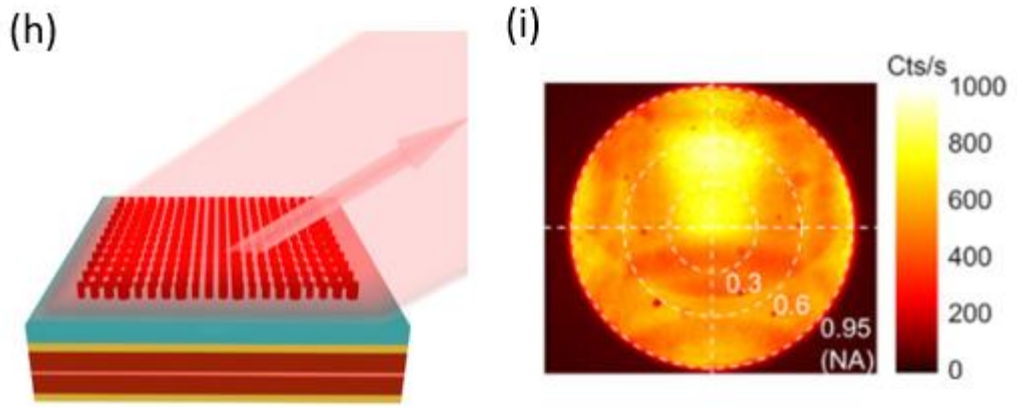

Figure 6. Light emission control using metasurfaces. (a) Illustration of metasurfaces controlling the wavefront of an external incident light with directionality. (b) Illustration of spontaneous emission from a light-emitting material. (c) Controlling light emission using metasurfaces by forming a photonic crystal cavity to attain directionality in in-plane direction. (d) Controlling light emission using metasurfaces by forming a closed cavity to attain directionality in out-of-plane direction. (e) Control of InGaN quantum well (QW) light emission using phased nanopillar array. (f) Top-view SEM image of the phased nanopillar array in (c). (g) Measured directional emission pattern from the InGaN QW with phased nanopillar array. (h) Control of GaN LED light emission using closed cavity and metasurface array. (i) Measured directional emission pattern from (f). (e) - (g) Reprinted with permission from [14], Copyright (2020) Nature Publishing Group; (h) and (i) Reprinted with permission from [15], Copyright (2019) Wiley-VCH.

Halide Perovskites as Novel Light-Emitting Materials

Of many novel light-emitting nanomaterials, halide perovskites are greatly advantaged due to its high photoluminescence quantum yield (PLQY), long-carrier diffusion length, and controllable bandgaps, low-cost and easy processing methods [16-18]. Lead Halide perovskites (ABX_3, A = MA^+, FA^+, or Cs^+; B = Pb^{2+}; X = Cl, Br or I), whose atomic structure is show in Figure 7, have been widely studied to achieve high efficiency LEDs [19-21] and lasers [22-25] across the visible spectrum. For some perovskites, their PLQY can be optimized to reach unity (100%) [26], which in turn is

highly energy-efficient as novel light sources. As the bandgaps of halide perovskites are tunable by changing the chemical composition, perovskites can be used as novel light sources across the whole visible spectrum. In most cases, its fabrication only involves the spin-coating of precursors. However, similar to many other light emitting materials, the control of light emission pattern still lacks developments, hindering its applications in many integrated smart lighting devices. In this thesis research, we aim to apply the 'closed cavity' approach in conjunction with phase gradient metasurfaces in order to directly control spontaneous light emission from a $CH_3NH_3PbI_3$ (Methylammonium lead iodide, $MAPbI_3$) perovskite layer.

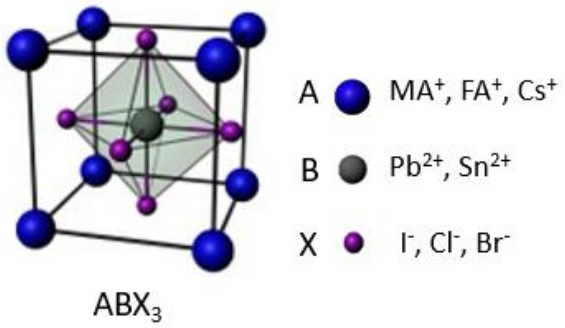

Figure 7. Crystal structure of metal halide perovskites.

It is worth noting that, while fabricating a simple perovskite thin film is facial, it is very difficult to integrate perovskite with metamaterials/nanostructures due to the fabrication constraints. This is attributed to the instability of perovskite in ambient air, especially in humid conditions. Besides, halide perovskites can be dissolved or degraded in many chemicals, which causes tremendous difficulty for lithography, in which many chemicals are used. Also, halide perovskites from spin-coating are easily degraded in high temperature environments, posing some difficulties to some thin-film deposition methods

in which some high-temperature processes are used. Last but not least, spin-coated perovskite layers do not have good surfaces roughness, which results in the difficulty of fabricating many other layers that might sit on top of the perovskite layer. However, in this thesis, all the aforementioned difficulties are solved, which is described in Chapter 3.

Design and Simulations of Several Perovskite-based Metastructures for Arbitrary Light Emission Wavefront Control

By sandwiching $MAPbI_3$ perovskite inside a Bragg resonant cavity, and apply dielectric metasurfaces on top of the cavity, arbitrary wavefront control of $MAPbI_3$ perovskite light emission can be achieved. Many devices with on-demand light emission pattern from $MAPbI_3$ perovskite can be enabled, including perovskite directional emitter, self-focused perovskite lens, perovskite vortex beam generator, etc. In this section, the design and simulations of these devices will be briefly presented.

In this thesis, all full device simulations are carried out using Lumerical FDTD Solutions (ANSYS Inc.), which solves Maxwell's equations with given geometry and optical properties in order to calculate the electric field distribution. In full device simulations, the light emission from $MAPbI_3$ perovskite is simplified as an in-plane dipole array centered at 770 nm wavelength ($MAPbI_3$ perovskite PL wavelength). The intensity of dipole array has a Gaussian distribution, which resembles the optical pumping intensity distribution in real optical measurements.

The design of a perovskite directional emitter is shown in Figure 8a, in which a perovskite emitting layer is sandwiched inside a cavity consisted of a Bragg multilayer reflector and a metallic bottom reflector. A phase-gradient metasurface that is designed to achieve anomalous refraction is placed on top of the cavity. The details of the phase-gradient metasurface for directional emitter will be discussed in Chapter 3. From full wave simulation, the far-field emission pattern shown in Figure 8b demonstrated a directional emission centered at 21° with respect to the surface normal.

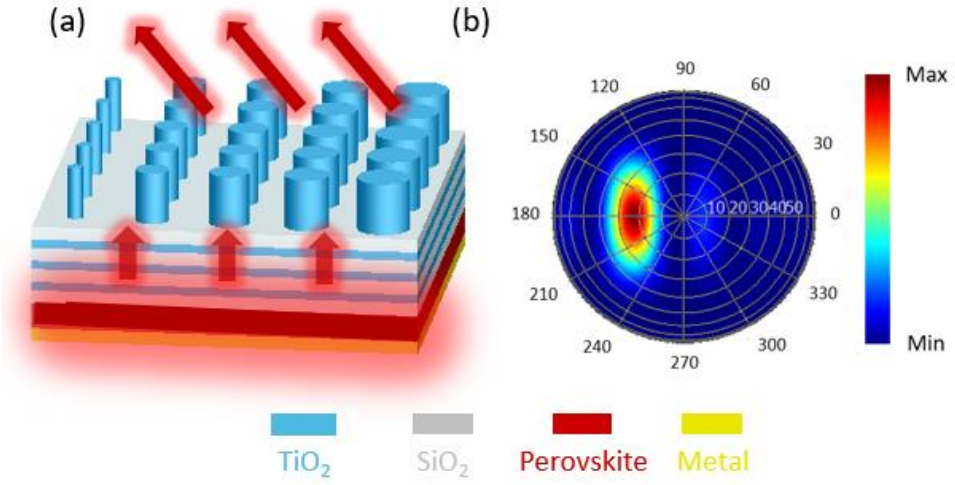

Figure 8. (a) Schematic and (b) simulated far-field radiation pattern of perovskite directional emitter.

In the design for self-focused perovskite emitting lens, the same cavity configuration is used. The metasurface, however, is spatially varied to achieve a focusing function, as shown in Figure 9a. Assuming the in-plane spatial coordinates (x, y) and the center of the metasurface is (0 ,0), the required phase at each position can be written as [27, 28]:

$$\Phi(x,y) = -(2\pi/\lambda)((x^2 + y^2)^{1/2} - f),$$

in which f is the focal length and λ is the wavelength of the light emission wavelength of perovskite. After constructing the focusing the metasurface, full wave simulation shows that the emitted light from perovskite layer focused at the designed focal length of f = 8 μm, as shown in Figure 9b.

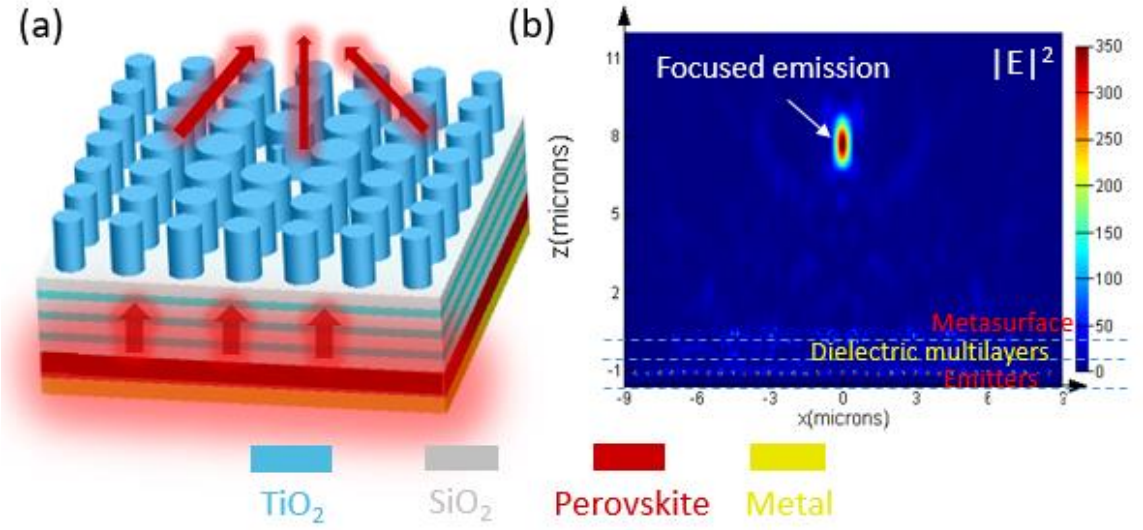

Figure 9. (a) Schematic and (b) simulated cross-section electric field intensity distribution of perovskite self-focused light emission lens.

The perovskite vortex beam generator again utilizes the same cavity configuration (Figure 10a). However, the metasurfaces are arranged such that the phase delay circularly increases [29, 30]. Figure 10b shows the top-view phase delay distribution, in which the metasurface is separated into 8 segments, and each segment provides gradually-increased phase gradient from 0 to 2π. By full wave simulation, a donut-shaped field distribution can be achieved from cut-plane electric field distributions, which is a characteristic field distribution for vortex beam generation [29, 30].

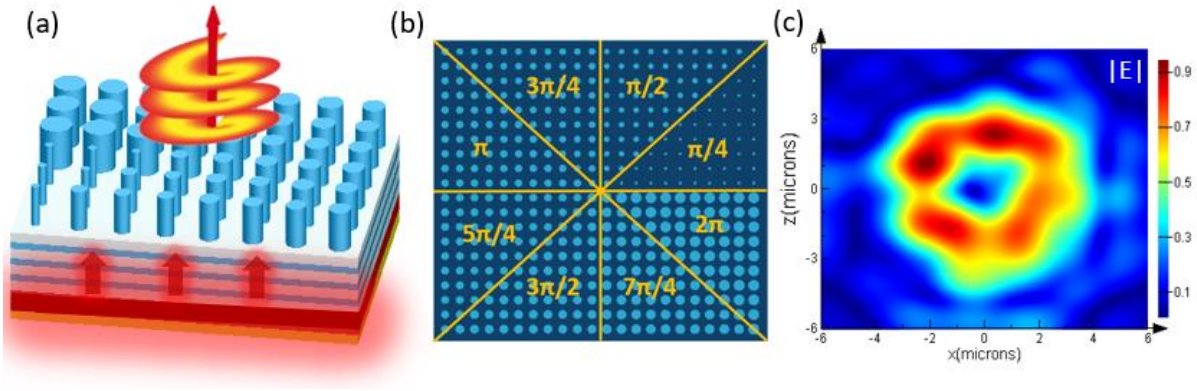

Figure 10. (a) Schematic and (b) top-view of the phase delay distribution and (c) simulated top-view electric field distribution of perovskite vortex beam generator.

References

[1] Kullock, René, et al. "Electrically-driven Yagi-Uda antennas for light." Nature communications 11.1 (2020): 1-7.

[2] Dregely, Daniel, et al. "3D optical Yagi–Uda nanoantenna array." Nature communications 2.1 (2011): 1-7.

[3] Kim, Jineun, et al. "Babinet-inverted optical Yagi–Uda antenna for unidirectional radiation to free space." Nano letters 14.6 (2014): 3072-3078.

[4] Ramezani, Mohammad, et al. "Hybrid semiconductor nanowire–metallic Yagi-Uda antennas." Nano letters 15.8 (2015): 4889-4895.

[5] Ho, Jinfa, et al. "Highly directive hybrid metal–dielectric Yagi-Uda nanoantennas." ACS nano 12.8 (2018): 8616-8624.

[6] Maksymov, Ivan S., Andrey E. Miroshnichenko, and Yuri S. Kivshar. "Actively tunable bistable optical Yagi-Uda nanoantenna." Optics express 20.8 (2012): 8929-8938.

[7] Kullock, René, et al. "Electrically-driven Yagi-Uda antennas for light." Nature communications 11.1 (2020): 1-7.

[8] Rahimi, Eesa, and Kürşat Şendur. "Temperature-driven switchable-beam Yagi-Uda antenna using VO2 semiconductor-metal phase transitions." Optics Communications 392 (2017): 109-113.

[9] Liu, Sheng, et al. "Light-emitting metasurfaces: simultaneous control of spontaneous emission and far-field radiation." Nano letters 18.11 (2018): 6906-6914.

[10] Cueff, Sébastien, et al. "Tailoring the local density of optical states and directionality of light emission by symmetry breaking." IEEE Journal of Selected Topics in Quantum Electronics 25.3 (2019): 1-7.

[11] Cui, Chengcong, et al. "Multiple Fano resonances in symmetry-breaking silicon metasurface for manipulating light emission." ACS Photonics 5.10 (2018): 4074-4080.

[12] Meng, Xiangeng, et al. "Unidirectional spaser in symmetry-broken plasmonic core-shell nanocavity." Scientific reports 3.1 (2013): 1-5.

[13] Rodriguez, S. R. K., et al. "Breaking the symmetry of forward-backward light emission with localized and collective magnetoelectric resonances in arrays of

pyramid-shaped aluminum nanoparticles." Physical review letters 113.24 (2014): 247401.

[14] Iyer, Prasad P., et al. "Unidirectional luminescence from InGaN/GaN quantum-well metasurfaces." Nature Photonics 14.9 (2020): 543-548.

[15] Khaidarov, Egor, et al. "Control of LED emission with functional dielectric metasurfaces." Laser & Photonics Reviews 14.1 (2020): 1900235. [16] Li, Yang, et al. "Orbital angular momentum multiplexing and demultiplexing by a single metasurface." Advanced Optical Materials 5.2 (2017): 1600502.

[16] Green, Martin A., Anita Ho-Baillie, and Henry J. Snaith. "The emergence of perovskite solar cells." Nature photonics 8.7 (2014): 506-514.

[17] Jena, Ajay Kumar, Ashish Kulkarni, and Tsutomu Miyasaka. "Halide perovskite photovoltaics: background, status, and future prospects." Chemical reviews 119.5 (2019): 3036-3103.

[18] Yin, Wan-Jian, et al. "Halide perovskite materials for solar cells: a theoretical review." Journal of Materials Chemistry A 3.17 (2015): 8926-8942.

[19] Lin, Kebin, et al. "Perovskite light-emitting diodes with external quantum efficiency exceeding 20 per cent." Nature 562.7726 (2018): 245-248.

[20] Wang, Nana, et al. "Perovskite light-emitting diodes based on solution-processed self-organized multiple quantum wells." Nature Photonics 10.11 (2016): 699-704.

[21] Xiao, Zhengguo, et al. "Efficient perovskite light-emitting diodes featuring nanometre-sized crystallites." Nature Photonics 11.2 (2017): 108-115.

[22] Sutherland, Brandon R., and Edward H. Sargent. "Perovskite photonic sources." Nature Photonics 10.5 (2016): 295.

[23] Saliba, Michael, et al. "Structured organic–inorganic perovskite toward a distributed feedback laser." Advanced Materials 28.5 (2016): 923-929.

[24] Zhang, Qing, et al. "Advances in small perovskite‐based lasers." Small Methods 1.9 (2017): 1700163.

[25] Huang, Can, et al. "Ultrafast control of vortex microlasers." Science 367.6481 (2020): 1018-1021.

[26] Liu, Feng, et al. "Highly luminescent phase-stable CsPbI3 perovskite quantum dots achieving near 100% absolute photoluminescence quantum yield." ACS nano 11.10 (2017): 10373-10383.

[27] Chen, Xianzhong, et al. "Dual-polarity plasmonic metalens for visible light." Nature communications 3.1 (2012): 1-6.

[28] Ni, Xingjie, et al. "Ultra-thin, planar, Babinet-inverted plasmonic metalenses." Light: Science & Applications 2.4 (2013): e72-e72.

[29] Yue, Fuyong, et al. "Vector vortex beam generation with a single plasmonic metasurface." ACS photonics 3.9 (2016): 1558-1563.

[30] Yu, Nanfang, et al. "Light propagation with phase discontinuities: generalized laws of reflection and refraction." science 334.6054 (2011): 333-337.

CHAPTER III

EXPERIMENTAL DEMONSTRATION OF A PEROVSKITE DIRECTIONAL EMITTER

Design of Perovskite Directional Emitter

The perovskite directional emitter applies a Bragg resonant cavity to sandwich a $MAPbI_3$ perovskite emitting layer, with a separately designed silicon (Si) metasurface on top, as shown in Figure 11. The Bragg cavity consists of a thin Ag film (25 nm) and 5 pairs of alternating TiO_2/SiO_2 layers, which shows 90% reflection at the photoluminescence wavelength of $MAPbI_3$ perovskite (770 nm). A silicon metasurface consists of silicon cylinders with spatially varying dimensions are used to achieve arbitrary wavefront control. Three germanium (Ge) layers of 4 nm-thick are used as interfacial adhesion promoting layer. Between the Ag film and the $MAPbI_3$ emitting layer, there is another layer of SiO_2 spacer to tune the resonance wavelength of the Bragg cavity to match the photoluminescence (PL) wavelength of $MAPbI_3$ perovskite. Unit cell design and full device simulations are conducted using a finite-difference time-domain full wave simulation package (Lumerical FDTD Solutions, ANSYS Inc.).

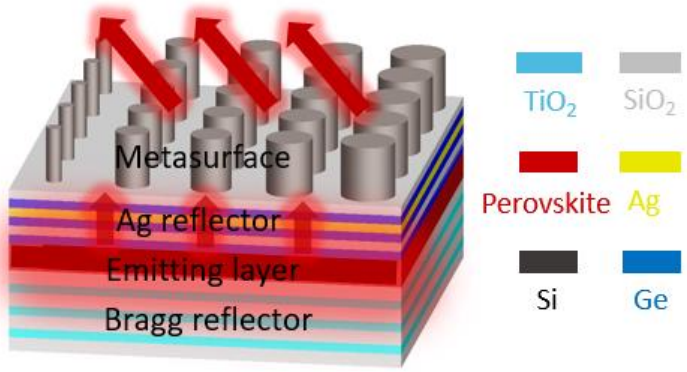

Figure 11. Schematic of a perovskite directional emitter.

The Bragg cavity is designed to operate at a resonant mode. The Bragg cavity consists of a TiO_2/SiO_2 distributed Bragg reflector (DBR) and a thin layer of Ag reflector. Alternating layers of high and low index dielectric materials can realize broadband high reflection due to the constructive multiple interference at each reflecting boundary. In this design, 60 nm-thick TiO_2 layers, whose refractive index n = 2.2 measured from a spectroscopic ellipsometer (EP3 Ellipsometer, Nanofilm), are used as the high refractive index layers. 160nm-thick SiO_2 layers are used as low index layers, whose refractive index n = 1.49, measured by ellipsometry. As shown in Figure 12, a total of 5 pairs of TiO_2/SiO_2 layers show a reflection of 90% at 770 nm wavelength, with a transmission of 90% at 532 nm wavelength, which is beneficial for the incidence of pump laser in a transmission mode. The reflection spectrum of the DBR is theoretically calculated based on ref. [1], and verified via two-dimensional FDTD simulations (Lumerical FDTD Solutions, ANSYS Inc.). Comparing to a resonance cavity with both metal reflectors, applying one DBR on one side also significantly reduces optical loss, as both TiO2 and SiO2 has negligible loss at the visible regime. A 25 nm-thick Ag film is used as the top reflector.

Ag is choosing as the metal material due to the fabrication constraints. The 25nm-thick Ag layer has a reflection of 60% and small amount of loss at 770 nm wavelength, which is enough for the operating of the resonant cavity. From the fabrication point of view, since the top reflector has to be deposited after the perovskite light emitting layer is spin-coated, it is best to reduce the number of layers, as well as the total deposition time above the perovskite layer, in order to reduce heating effects and perovskites' exposure to the ambient air. Therefore, comparing to using another DBR, which would require a multilayer electron beam deposition on top of perovskite for a few hours, using a thin Ag reflector is a better choice while not compromising the performance of the perovskite directional emitter devices.

In order to match the emission wavelength to the narrow resonant cavity wavelength, a lossless SiO_2 spacer is sandwiched in between Ag and perovskite layers. By FDTD numerical simulation, the spacer thickness is optimized at 150 nm. The cavity transmission is shown in Figure 12b, in which a resonant peak can be observed centered at 770 nm, which is the characteristic resonance peak of Bragg cavities.

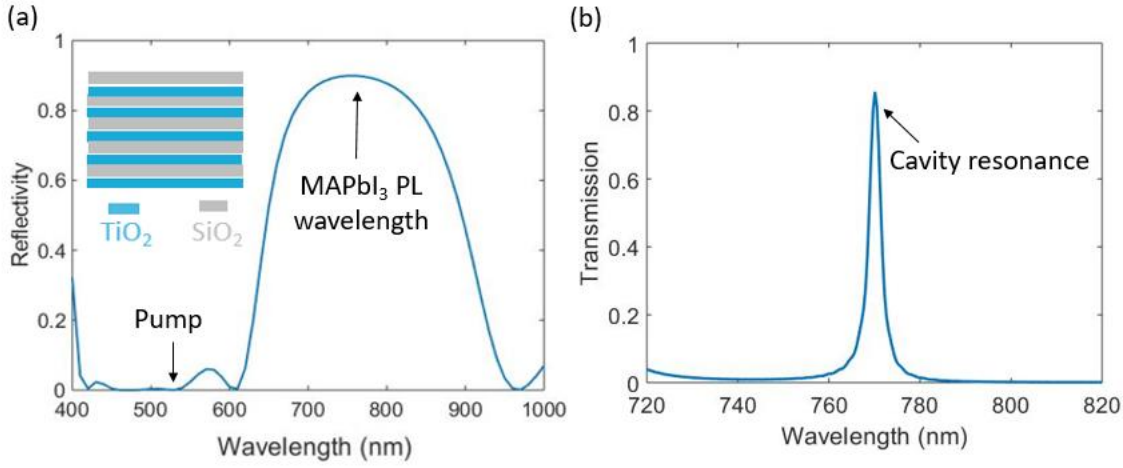

Figure 12. (a) Design of the distributed Bragg reflector (DBR). Reflection reaches 90% at 770nm. (b) Design of the Bragg resonant cavity. A resonant peak is observed at 770nm.

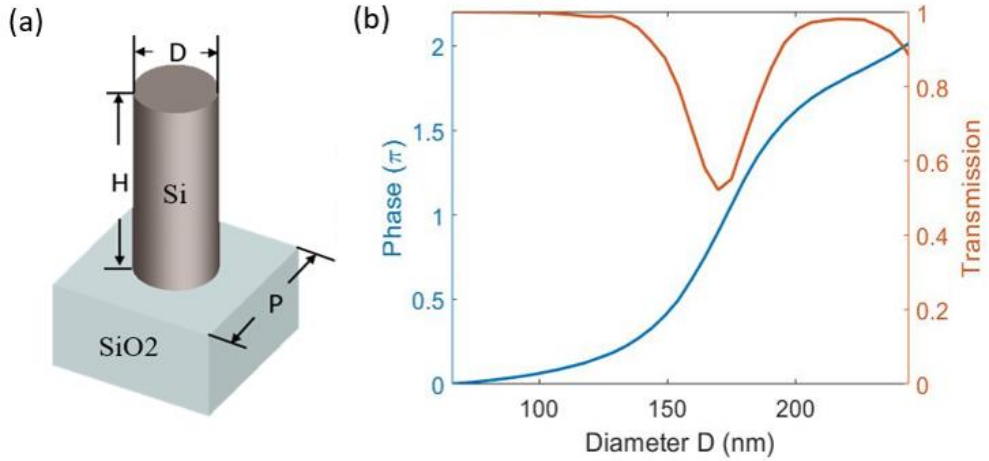

Figure 13. (a) Design of the silicon metasurface unit cell. Period P = 330nm, height H = 325 nm are used to achieve 2π phase shift. (b) Calculation of the accumulated phase shift and transmission of the unit cell with varying diameters D of the silicon cylinders.

The unit cell of the dielectric metasurface is shown in Figure 13a. A silicon cylinder of height *H* = 325 nm and diameter *D* sits on top of a glass substrate. The period

of unit cell is fixed at P = 330 nm. Silicon is used as a dielectric metasurface material due to its high refractive index (n = 3.7) and low absorption at $MAPbI_3$ photoluminescence wavelength (770 nm). There are a few considerations in choosing silicon as the metasurface material. First, from the design point of view, silicon has a high refractive index, which is idea for dielectric metasurfaces, in which a high-refractive index material is needed to attain sufficient phase delay upon an impinging plane wave with a thin layer of structure. Besides, silicon also has low (but not negligible) loss at the perovskite light emission wavelength of 770 nm, which can be seen from the transmission plot in Figure 13b. Furthermore, it is feasible to use low-temperature electron beam evaporation to deposit the silicon layer. There are other high-index dielectric materials that have low losses in the visible regime, with the most notable being TiO_2 [2] and GaP [3]. However, for both materials, the deposition of them on the perovskite would be troublesome with the presence of high temperature and/or humid environments. Therefore, it is best to use poly-Si deposited from electron-beam evaporation as the metasurface materials for out purposes.

Table 1 Phase delays and diameters of the 6 silicon cylinders within one supercell.

Unit cell No.	**1**	**2**	**3**	**4**	**5**	**6**
Phase delay (rad)	π/3	2π/3	π	4π/3	5π/3	2π
Diameter (nm)	145	162	172	185	205	244

As mentioned in Chapter 1, in order to achieve full arbitrary phase control, 2π phase delay by varying the dimensions of the silicon cylinder is needed. Full 2π phase

delay is achieved by varying the diameter *D* of the silicon cylinders (Fig. 3a). High transmission (>0.5) is maintained across the whole diameter variation in order to achieve high efficiency (Fig. 11b).

In order to design a perovskite directional emitter, the silicon metasurface is designed to realize anomalous refraction [29]. By spatially varying the diameters of silicon cylinders, different phase delay of the propagating wavefront can be introduced. When the wavefront phase delay is arranged to have a constant gradient, a phase delay term is essentially added to the Snell's law. The generalized form of Snell's law then could be written as [29]:

$$\sin(\theta_t)n_t - \sin(\theta_i)n_i = (\lambda/2\pi)(d\varphi/dx)$$

where θ_i and θ_t is the incident angle and refracted angle, respectively, while n_i and n_t are the refractive indices of the incident and transmission medium, respectively. By arranging 6 unit cells in a supercell, whose diameters and transmission coefficients are shown in Table 1, an anomalous refraction of 23° can be achieved. Therefore, by applying the metasurface on top of the perovskite emission cavity, a directional emission of 23° can be achieved. Full device simulation is carried out using Lumerical FDTD Solutions (ANSYS Inc.). As shown in the simulated far-field radiation intensity-angle distribution in Figure 14, the perovskite directional emitter shows the emitted light centered 23° to the left.

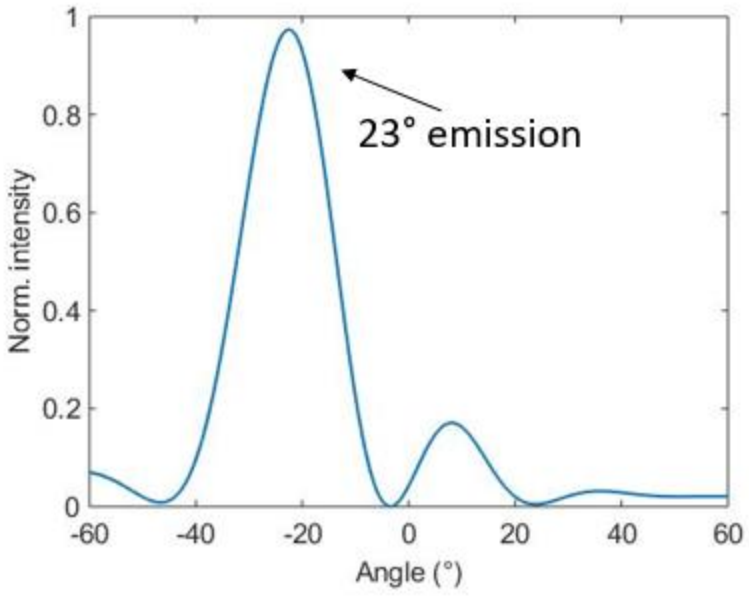

Figure 14. Calculated Far-field emission profile from the perovskite directional emitter with a designed 23° emission.

Fabrication Process and Considerations

As mentioned in Chapter 2, since halide perovskites are unstable in ambient environment and easily degraded by many chemicals, the fabrication of perovskite-based nanostructures and metamaterials are difficult. Therefore, the fabrication process of the perovskite light emitting metamaterial is sophistically optimized. In this section, considerations to optimize the fabrication process will be discussed.

To avoid long-time multilayer electron beam deposition, a distributed Bragg reflector (DBR) consisting of TiO_2/SiO_2 multilayer would be first deposited on a glass substrate by electron beam evaporation (Lesker PVD 75 E-beam Evaporator) (Step i). The deposition rate for TiO_2 is 0.15 nm/s, and for SiO_2 the deposition rate is 0.25 nm/s.

Between each layers, 10-minutes waiting periods are applied to allow the evaporator chamber to cool down.

Before spin-coating $MAPbI_3$ perovskite, the deposited multilayer is cleaned again using acetone, Isopropyl alcohol (IPA) and deionized (DI) water, followed by UV-Ozone treatment of 15 minutes. 1.7 M $MAPbI_3$ solution is prepared by mixing equimolar MAI and PbI_2 in DMF:DMSO (VDMF:VDMSO = 9:1) and stirring for 30 minutes. Then the solution is filtered by 0.22 μm pore size filters. The perovskite solution is spin-coated at 3000 rpm for 25 seconds, and 400 μl diethyl ether is dropped onto the precursor film (after 10 seconds spin-coating) and followed another continuous 15 seconds spin-coating. The sample is then heated by gradient annealing, with 65 ℃ for 1 minute and 100 ℃ for 10 minutes in order to complete the crystallization. (Step ii) The thickness of the $MAPbI_3$ layer is measured to be 600 nm by a stylus-based surface profilometer (Dektak). The spin-coated $MAPbI_3$ perovskite is shown in the image in Figure 15, in which a clear mirror-like surface can be seen.

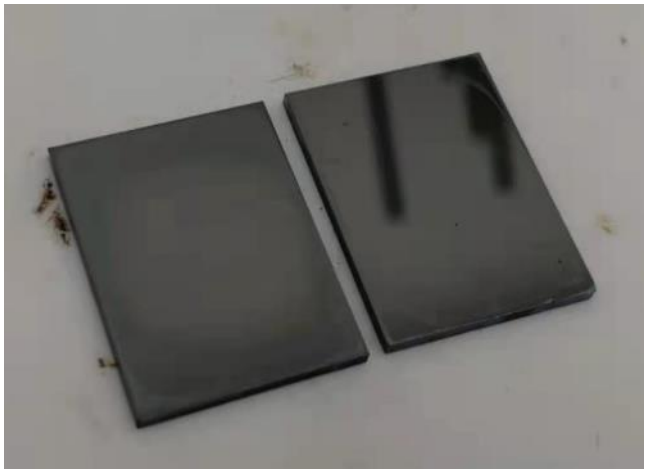

Figure 15. Spin-coated $MAPbI_3$ perovskite with mirror-like surfaces.

Three layers of Ge (4 nm thick for each layer, 0.05 nm/s), 150 nm SiO_2 spacer (0.25 nm/s), 25 nm Ag reflector (0.2 nm/s) and 325 nm Si (0.15 nm/s) layer are subsequently deposited by electron-beam evaporation (Step iii). Another 100nm-thick SiO_2 is also deposited between Ag and Si as an etch stop layer. Ge adhesion layers are used to promote the interfacial between rough $MAPbI_3$ perovskite layer and SiO_2 layer, as well as between SiO_2 and Ag layers. Since in Step iii, all the deposition processes are carried out with the presence of $MAPbI_3$ perovskite, it is crucial to control the temperature of the e-beam evaporator chamber. The temperature inside the chamber is monitored, with many waiting periods applied to prevent the chamber temperature elevating to over 80 ℃.

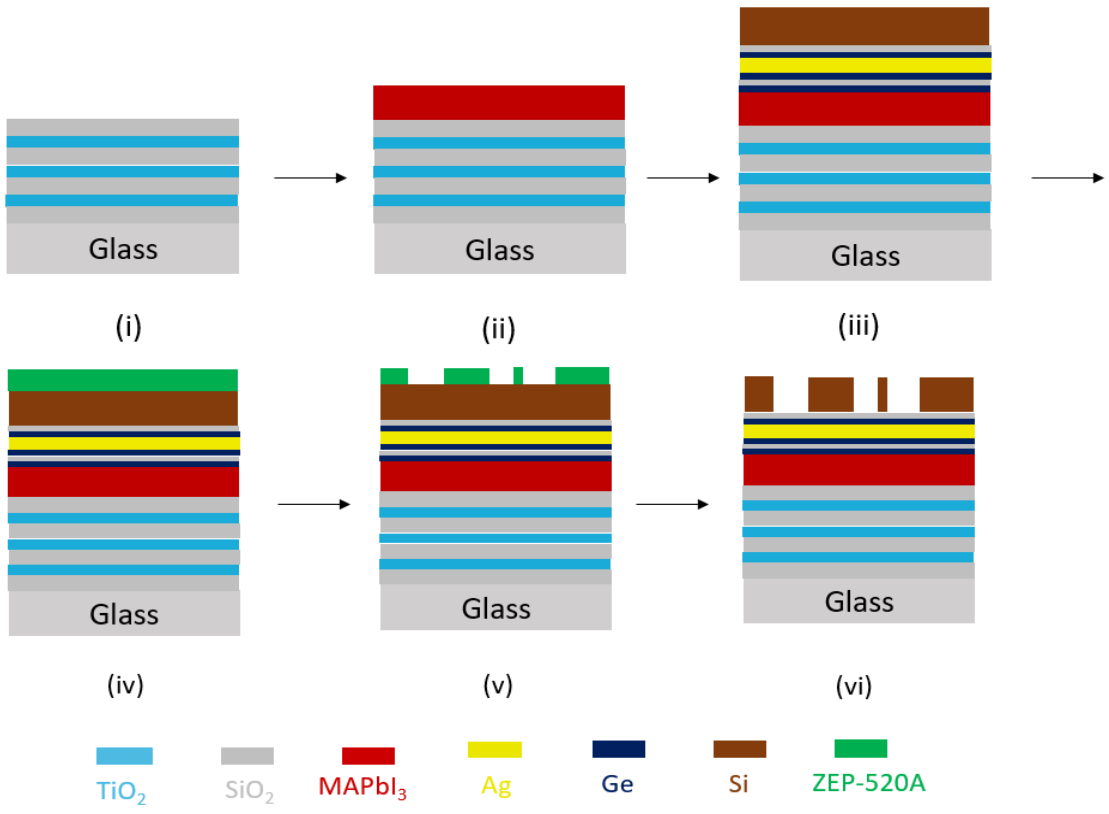

Figure 16. Optimized fabrication process of perovskite directional emitter metamaterials.

In order to pattern the silicon metasurface, a proper electron beam lithography with dry-etching recipe needs to be selected. From the etching point of view, either metallic hard etch mask or electron beam resist etch mask can be potentially used. However, since almost all solutions that can be used to remove thin metallic layers will degrade perovskite, electron-beam resist has to be directly used as etch mask. Besides, during the eletron beam lithography and the subsequent developing process, the solutions used need to be perovskite-friendly and water-free. Among most electron-beam resists that have good dry-etching resistance, ZEP-520A electron beam resist (ZEON Chemicals) is the best choice, whose developer ZED-N50 (ZEON Chemicals) is also water-free. Directly electron-beam patterning on lead halide perovskites using ZEP-520A as electron beam resist has also been reported [4]. The inverse pattern of the metasurface is then exposed by 30kV electron-beam lithography (Tescan MIRA) on a 300 nm (spin-coated at 5500 rpm) thick positive tone ZEP-520A resist (Step iv), followed by developing in ZED-N50 developer for 2 minutes (Step v), and rinse in IPA for 30 seconds. Finally, extreme cautions were taken to blow dry the sample using N_2.

Resist pattern is transferred to the metasurface by induced coupled plasma etching (Oxford Plasmalab 100) with a CHF_3/SF_6 gas mixture at 20 mTorr. The flow rates for CHF_3 and SF_6 are 75 sccm and 15 sccm respectively, which are optimized to achieve a ZEP-520A:Si selectively of 1:2.5. The etching gas mixture has high $Si:SiO_2$ selectivity, since SiO_2 is used as an etch stop layer underneath the Si metasurface. After etching, remaining ZEP-520A resist are removed by O_2 plasma (Step vi). All fabrication process

is completed in AggieFab Nanofabrication Facility in Texas A&M University. The fabricated device is shown in the scanning electron microscope (SEM) images in Figure 17.

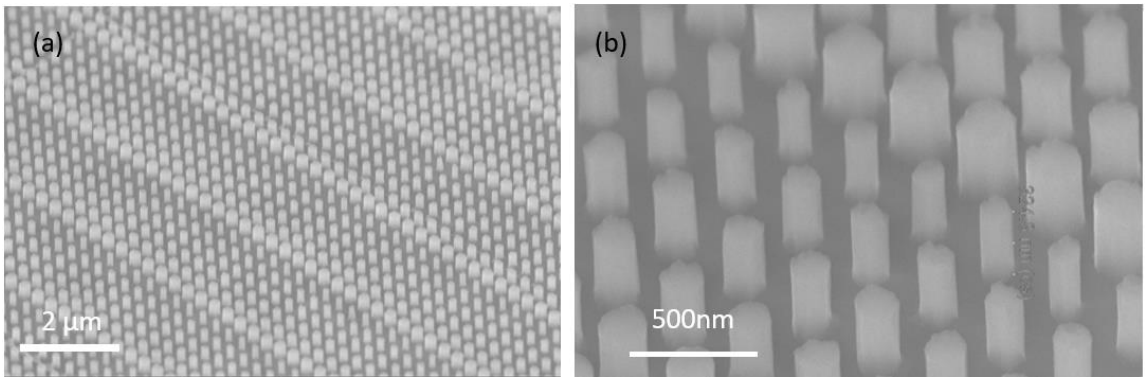

Figure 17. SEM images of fabricated perovskite directional emitter.

Optical Measurement Results

The fabricated perovskite metamaterial is characterized using an in-house momentum-resolved photoluminescence measurement setup (Figure 18). The pump beam from a Ti:Sapphire laser (Chameleon Ultra II, Coherent Inc.) is fixed at 532nm wavelength, at which the bottom DBR of perovskite metamaterial has >90% transmission. A variable attenuator is used to adjust the pump power, which is measured to be 1µW in the experiments. The light emission from $MAPbI_3$ perovskite metamaterial (centered at 770nm) is collected in transmission mode by an objective lens (M Plan Apo 50X, 0.55 NA, Mitutoyo). A long-pass filter (cutoff wavelength 700nm, Thorlabs) is then used to block the pump laser, only allowing the emitted light from perovskite to be collected by the charge-coupled camera (CCD) camera and spectrometer. The back focal plane (Fourier plane) of the emitting sample surface is then projected to a CCD camera (PIXIS, Princeton

Instruments). The photoluminescence spectrum of perovskite light emission is then measured by a spectrometer (SpectraPro HRS-300, Princeton Instruments).

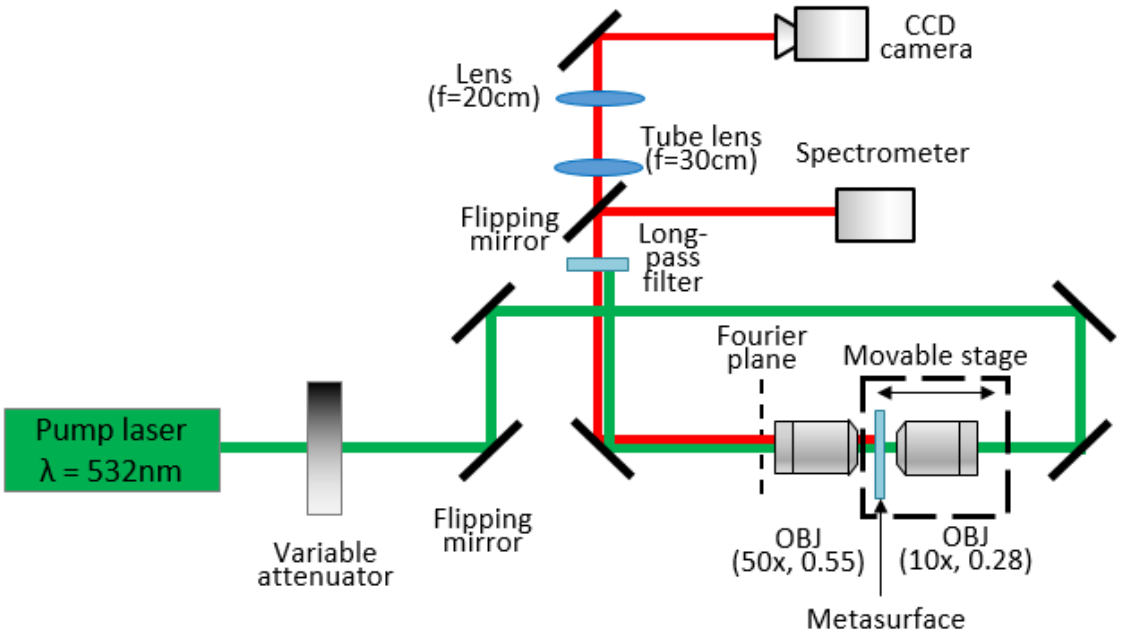

Figure 18. Optical measurement setup of perovskite directional emitter metamaterials.

Figure 19 shows the measured the photoluminescence (PL) spectrum before and after the optical measurements. The PL peak is measured to center at 770nm. The black curve was taken before the measurement, while the red curve was taken after optical measurement in ambient air for a few hours subject to laser radiation. After the measurement, the PL peak intensity only dropped 30%, which shows that the $MAPbI_3$ perovskite directional emitter has good stability in ambient air under laser pumping.

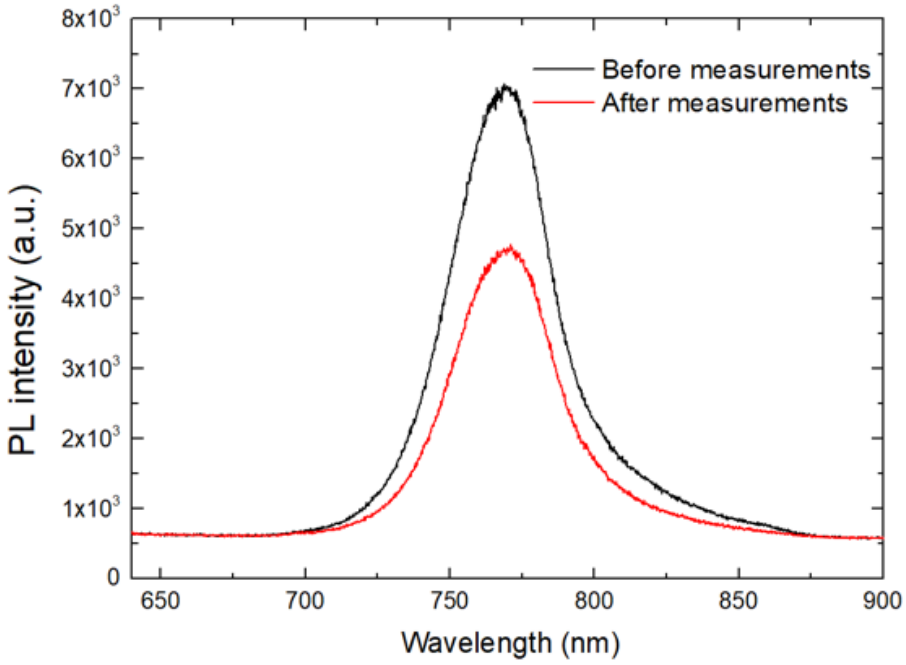

Figure 19. Photoluminescence spectrum of $MAPbI_3$ perovskite directional emitter before (black line) and after (red line) optical measurement.

The momentum-resolved PL is shown in Figure 20, in which the x-axis shows the directional emission angle in the momentum space, while y-axis shows the wavelength. It is clear that the PL from $MAPbI_3$ perovskite has a directional emission at (k_x/k_0 = -0.39, which corresponds to 23° directional emission with respect to the surface normal direction.

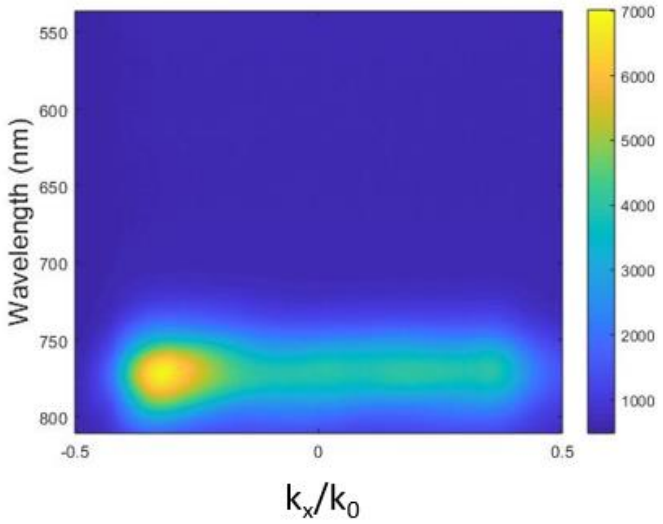

Figure 20. The momentum-resolved PL spectrum of the $MAPbI_3$ perovskite directional emitter.

The effects of using dielectric metasurface is shown in Figure 21. In Figure 21a, the light emission pattern from outside the metasurface region is demonstrated. Without any patterns, the measured momentum space image of the emitted light at 770 nm shows a broad and normal direction emission to the sample surface. In comparison, with the presence of the metasurface, directional emission at 23° is achieved (k_x/k_0 = -0.39), as shown in the momentum space image in Figure 21b. The emission pattern agrees well with the simulated far-field pattern (Figure 14), confirming the design principle of the perovskite metamaterial directional emitter.

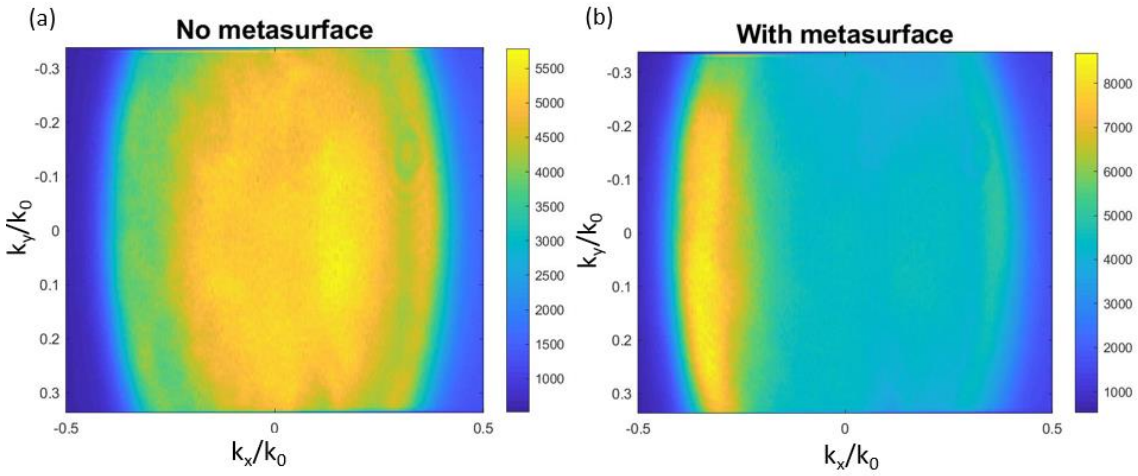

Figure 21. (a) Measured momentum-space image from perovskite without a metasurface. (b) Measured momentum-space image from the perovskite directional emitter, showing 23° angled emission.

References

[1] Wartak, Marek S. Computational photonics: an introduction with MATLAB. Cambridge University Press, 2013.

[2] Khorasaninejad, Mohammadreza, et al. "Metalenses at visible wavelengths: Diffraction-limited focusing and subwavelength resolution imaging." Science 352.6290 (2016): 1190-1194.

[3] Melli, Mauro, et al. "Gallium phosphide optical metasurfaces for visible light applications." Scientific Reports 10.1 (2020): 1-7.

[4] Zhang, Chen, et al. "Lead Halide Perovskite‐Based Dynamic Metasurfaces." Laser & Photonics Reviews 13.7 (2019): 1900079.

CHAPTER IV

CONCLUSIONS AND OUTLOOK

In conclusion, this thesis has demonstrated the method to utilize Bragg resonant cavity and dielectric metasurface integrated with a novel perovskite light emitting materials to achieve on-demand and arbitrary light emission wavefront control. The perovskite-based light-emitting metastructure devices enable many desired light emission patterns, including directional emission, self-focused light emission, as well as vortex beam generation. The devices are potentially energy-efficient, low-cost, easy-processing, and tunable, thanks to the advantages of halide perovskites.

Experimentally, a perovskite directional emitter is successfully fabricated. The fabrication difficulties in integrating unstable halide perovskite into metastructures have been solved by carefully optimizing the fabrication workflow. From optical measurements, controllable directional light emission from $MAPbI_3$ perovskite has been demonstrated and matched the designed emission angle very well. The device can be used as a compact integrated novel perovskite based light source. This can also be beneficial for many perovskite-based applications, such as directional LEDs, light detection and ranging, optical communications, etc.

On the other hand, phase-gradient metasurfaces have mostly been applied to control the wavefront of externally incident light. However, in this thesis, metasurfaces are utilized to control the light generation from the metastructure itself. We envision that this thesis also expands the horizon of applications of metasurfaces.

In the future research, first, it is important to experimentally realize more functionalities from perovskite light emission, including focused light emission, light emission from perovskite with orbital angular momentum, and perovskite self-emitted holograms, etc. Besides, it is also exciting to incorporate the arbitrary wavefront control capability with perovskite-based optoelectronic devices. For example, the directional emitter can be integrated with perovskite LEDs and experimentally demonstrated, facilitating directional perovskite LEDs. Furthermore, with the advances of micro/nanoscale 3D printing, it is also interesting to experimentally explore three-dimensional wavefront control of perovskite light emission. Last but not least, active control of perovskite light-emission with reconfigurable metasurfaces would also be interesting to be experimentally explored.